was reinserted (at WB_1), the pressure jumped to P(RR), indicating the formation of an RR. The pressure then dropped suddenly to P(MR), again indicating a spontaneous transition from a regular to a Mach reflection. The process was repeated at WR_2. Consequently, the stable reflection for $\omega_i = 34.8$ deg is again an MR.

In spite of the similarity just described in the observed processes in Figs. 2b and 2c, there was one noticeable difference between them, namely the time duration of the existence of the RR from the moment of its formation (at WB) until its spontaneous transition to a Mach reflection. Whereas, as can be seen in Fig. 2b, the four transient regular reflections, which were formed at WB_1, WB_2, WB_3, and WB_4, lasted for about 18, 9, 4, and 18 s, respectively, the two transient regular reflections, which were formed at WB_1 and WB_2 (see Fig. 2c), existed for about 60 and 55 s, respectively. Consequently, it is apparent from Figs. 2a–2c that as ω_i approached the value appropriate for the transition from a stable MR to a stable RR, the duration of the transient RR increased.

A different sequence of events is evident in Fig. 2d for $\omega_i = 34.0$ deg. The pressure appropriate to the initially established Mach reflection P(MR) jumped, as expected, to P(OS) when the lower wedge was removed (at WR_1). When the lower wedge was reinserted (at WB_1), the pressure jumped to P(RR), indicating the establishment of an RR. However, unlike the cases recorded in Figs. 2a–2c, the RR this time was stable and did not change spontaneously to a Mach reflection. Once an RR was established, the removal of the lower wedge (at WR_2) resulted in a drop in the pressure from P(RR) to P(OS), and the return of the lower reflecting wedge, at WB_2, resulted in a jump back to P(RR). Hence, based on the results shown in Fig. 2d the stable reflection for $\omega_i = 34.0$ deg is an RR. In summary, the results shown in Figs. 2a–2d indicate that Mach reflection wave configurations were stable for $\omega_i \geq 34.8$ deg and that RR wave configurations were stable for 34.0 deg. Averaging between these two values results in $\omega_i^{cr} \approx 34.4$ deg, in contrast to the value obtained in Ref. 1, i.e., $\omega_i^{cr} = 35.5$ deg, which was based on continuous (video) photography.

The reason for the formation of a transient RR before the establishment of a stable MR for $\omega_i > \omega_i^{cr}$ is understood if one inspects the numerical simulation of the evolution of an MR as shown in Fig. 3, which is taken from Ref. 4. As can be seen, the oblique shock wave, which is formed at the leading edge of the wedge, reflects first at the symmetry line as an RR (see Figs. 3a and 3b). This RR then changes to a Mach reflection (Fig. 3c), which after a while reaches its steady-state position and configuration.

Based on the numerical simulation shown in Fig. 3, one can conclude that even when the initial conditions are appropriate to a stable MR the evolution to the stable MR starts with a transient RR. When $\omega_i \gg \omega_i^{cr}$, as is the case in Fig. 2a, the duration of the transient RR is extremely short. In fact, it is so short that sometimes it is not even recorded. However, as ω_i approaches ω_i^{cr}, as is the case in Figs. 2b and 2c, the duration of the existence of the transient RR increases. The mechanism(s) causing the termination of the RR in this case is(are) yet to be understood.

Conclusions

The stability of RR and MR in the dual solution domain was investigated experimentally. A pressure-measurement-based method was applied.

It was found that the dual solution domain, i.e., $\omega_i^{tr}(\mathrm{MR} \rightarrow \mathrm{RR}) \leq \omega_i \leq \omega_i^{tr}(\mathrm{RR} \rightarrow \mathrm{MR})$, is divided by a critical angle, say, ω_i^{cr}, into two subdomains. RR is stable in the subdomain $\omega_i^{tr}(\mathrm{MR} \rightarrow \mathrm{RR}) < \omega_i < \omega_i^{cr}$, and MR is stable in the subdomain $\omega_i^{cr} < \omega_i < \omega_i^{tr}(\mathrm{RR} \rightarrow \mathrm{MR})$.

In addition, it was found that even when the stable wave configuration is an MR, it was preceded, in the vicinity of the critical angle ω_i^{cr} by a transient RR wave configuration that spontaneously changed to an MR. The average duration of the temporal regular reflection was found to increase as the value of ω_i^{cr} was approached from above. At the flow Mach number $M_0 = 4.96$, it was found that $\omega_i^{tr}(\mathrm{MR} \rightarrow \mathrm{RR}) = 30.9$ deg, $\omega_i^{tr}(\mathrm{RR} \rightarrow \mathrm{MR}) = 37.2 < \omega_i^{D} = 39.3$ deg, and $\omega_i^{cr} \approx 34.4$ deg, in contrast to the value 35.5 deg, which was reported previously. The average time duration of the existence of the transient regular reflections Δt was found to be 0 for $\omega_i \geq 38.6$ deg, 12.5 s for 35.1 deg, 57.5 s for 34.8 deg, and $\rightarrow \infty$ for ≤ 34.4 deg. Finally, both $\omega_i^{tr}(\mathrm{RR} \rightarrow \mathrm{MR})$ and ω_i^{cr} depend on the dimensions of the wedges.

Acknowledgment

The authors would like to thank J.-C. Lengrand, director of Laboratoire d'Aerothermique, for his constructive comments in the course of this study.

References

[1]Chpoun, A., Passerel, D., Li, H., and Ben-Dor, G., "Reconsideration of Oblique Shock Wave Reflections in Steady Flows, Part I, Experimental Investigation," *Journal of Fluid Mechanics*, Vol. 301, 1995, pp. 19–35.

[2]Vuillon, J., Zeitoun, D., and Ben-Dor, G., "Reconsideration of Oblique Shock Wave Reflections in Steady Flows, Part II, Numerical Investigation," *Journal of Fluid Mechanics*, Vol. 301, 1995, pp. 37–50.

[3]Ben-Dor, G., *Shock Wave Reflection Phenomena*, Springer–Verlag, New York, 1991.

[4]Vuillon, J., Zeitoun, D., and Ben-Dor, G., "Numerical Investigation of Shock Wave Reflection in Steady Flows," *AIAA Journal*, Vol. 34, No. 6, 1996, pp. 1167–1173.

Correlation of Separation Angles Induced by Glancing Interactions

S. Koide*
Japan Defense Agency, Tokyo 190, Japan
and
N. Saida† and R. Ogata‡
Aoyama–Gakuin University, Tokyo 157, Japan

Introduction

GLANCING shock-wave/turbulent-boundary-layer interaction, in which an oblique shock wave glances across a boundary layer growing along an adjacent wall (see Fig. 1), constitutes one of the most important phenomena of three-dimensional interference. Several studies of this phenomenon have been conducted recently with the objective of correlating the glancing-interaction features induced by unswept sharp fins (USF) at different Mach numbers with various wedge angles,[1] and subsequently deducing relationships between the interactions produced by several geometrically dissimilar shock generators such as USF, swept sharp fins, and semicones (SC).[2] The families of swept sharp fins and SC induce conical inviscid shock waves, which have curvature, whereas the USF induces a planar shock wave. However, in most of the previous studies, shock-wave strength given solely by inviscid shock angle has been considered to correlate the interaction features even when the types of shocks differ.

In this study, angles of primary separation lines induced by three disparate families of shock generators (Fig. 1)—USF, SC, and swept triangle fins (STF)—are emphasized, and relationships among the three families are investigated by considering the inviscid pressure field in the interaction region. A correlation law useful for predicting the separation angles, which takes into account the shock-curvature effect, is then postulated.

Received March 19, 1996; revision received June 25, 1996; accepted for publication June 25, 1996; also published in *AIAA Journal on Disc*, Volume 2, Number 1.

*Senior Research Engineer, 2–5th Laboratory, Third Research Center, Technical R&D Institute, 1-2-10 Sakae, Tachikawa. Member AIAA.

†Professor, Department of Mechanical Engineering, College of Science and Engineering, 6-16-1 Chitosedai, Setagaya.

‡M.S. Student, Department of Mechanical Engineering.

Primary Separation Lines and Their Angles

The primary separation line is one of the most easily discerned features of the interaction footprint obtainable by surface flow visualization. The separation angle β_s is defined as the angle formed by the primary separation line and the incoming freestream direction. For the cases of USF and SC, experimental data sets are available.[1-5] For STF, parametric experiments have been carried out at Aoyama–Gakuin's 8×10 cm^2 supersonic wind tunnel using STF with $\alpha = 12$, 18, and 24 deg and $\lambda = 15$, 30, and 45 deg. All tests were conducted at $M = 2.50 \pm 1.2\%$, $Re = 3.74 \times 10^7/\text{m} \pm 3.0\%$ and under nearly adiabatic wall-temperature conditions. The test boundary layer, whose thickness δ was 5.0 mm, was fully turbulent with very little spanwise variation. All STF employed in the present study have an α remarkably smaller than 90 deg $- \lambda$). Hence the geometry is treated as a fin rather than as a swept compression corner. Details of these experiments are described elsewhere.[6]

Angles of Shock Waves and Pressure Increases Across the Shocks

To correlate β_s caused by disparate shock generators, previous investigations[2] have employed the angle of the inviscid shock trace on the test surface β_o (Fig. 1); β_o can be calculated easily for USF and SC, using oblique shock theory and Taylor–Maccoll theory, respectively. For STF, a shock-angle-prediction method developed by Koide et al.[7] can provide β_o for wide ranges of α, λ, and M.

In addition to the shock angle, inviscid pressure rise across the shock has been calculated for USF, SC, and STF to consider the shock-curvature effect. Figure 2 presents an example of the corresponding pressure rise along a line labeled Y. The three cases were calculated for a constant β_o (31.7 deg) at a fixed M (2.46). Pressures for USF and SC were calculated using the same theories applied for β_o, whereas an Euler computational fluid dynamics (CFD) solver developed by Griesel[7,8] was employed for STF. Because the CFD solver is based on a shock-capturing method, the STF inviscid shock has a certain width. Hence, a finite pressure gradient exists at the STF shock location. To create the same β_o under a fixed M, the half-apex (or wedge) angle α must be increased as the radius of the shock curvature decreases (USF → STF → SC).

In the case of planar shock induced by USF, the pressure rise across the shock takes the form of a step. But in the case of conical shock, to which SC and STF belong, the pressure behind the shock increases gradually toward the generator surface because of the conical nature of the flow. Because β_o remains constant, the pressure just behind the shock, PR_o, remains constant and, for a specific-heat ratio of 1.4, is $(7M^2 \sin^2 \beta_o - 1)/6$. (In the following, PR indicates a nondimensional pressure divided by the undisturbed incoming pressure.) The difference between PR_o and the overall pressure rise PR_{oa} (Fig. 2) tends to increase with decreasing radius of shock curvature. This difference should have a certain influence when the shock interacts with a boundary layer.

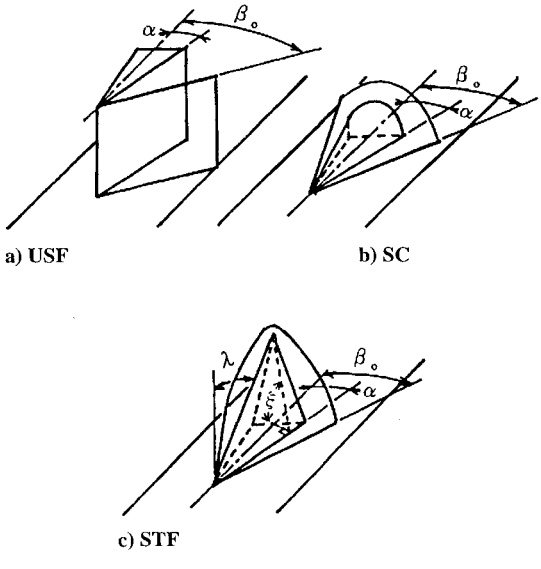

Fig. 1 Schematic views of several types of glancing interactions.

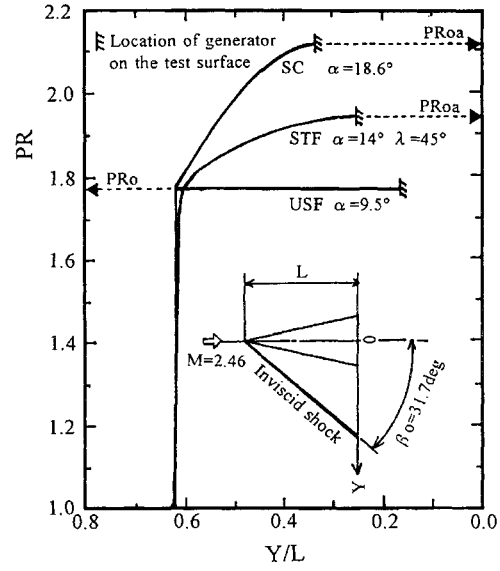

Fig. 2 Inviscid pressure increases across the shock waves induced by USF, SC, and STF, calculated for $\beta_o = 31.7$ deg at $M = 2.46$.

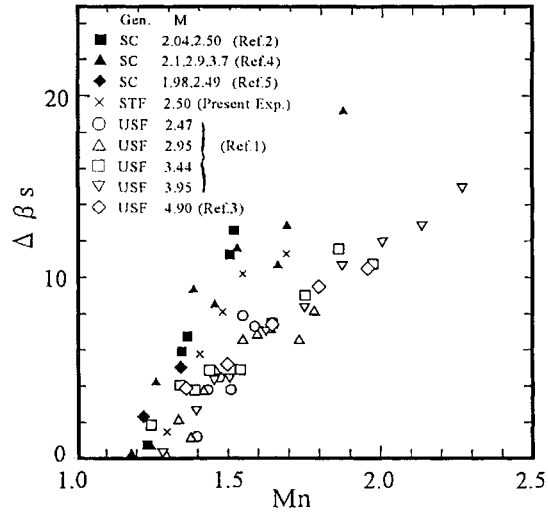

Fig. 3 Correlation of the separation angles in terms of β_o and M_n.

Correlation of Separation Angles

Using the separation angles and the inviscid-flow features described above, the correlation of β_s with the inviscid flowfield was investigated. Figure 3 shows, in $\Delta\beta_s (\equiv \beta_s - \beta_o)$ and $M_n (\equiv M \sin \beta_o)$ coordinates, a comparison between angles of β_s induced by the three families of shock generators. USF (open symbols) show tendencies different from SC (solid symbols). Data points for STF (labeled ×) are located between those for USF and SC. In Fig. 3, β_o and M are the only parameters taken into account in the correlation. However, as remarked in Fig. 2, the shocks resulting from USF, SC, and STF have different curvatures, and induce different behavior of the inviscid-pressure rise. The data correlation of Fig. 3 is shown to be improved when the curvature effect is taken into account.

To introduce the curvature effect, attention was focused on the overall pressure rise PR_{oa} shown in Fig. 2. For SC, PR_{oa} can be obtained by applying Taylor–Maccoll theory. Unlike the case of SC, PR_{oa} cannot be found using a known simple method for STF. However, the same correlation procedure developed for predicting averaged pressure rise for STF[8] also can be used to obtain PR_{oa}. Using computed values of PR_{oa} for STF with $8 \leqq \alpha \leqq 17$ deg, $30 \leqq \lambda \leqq 60$

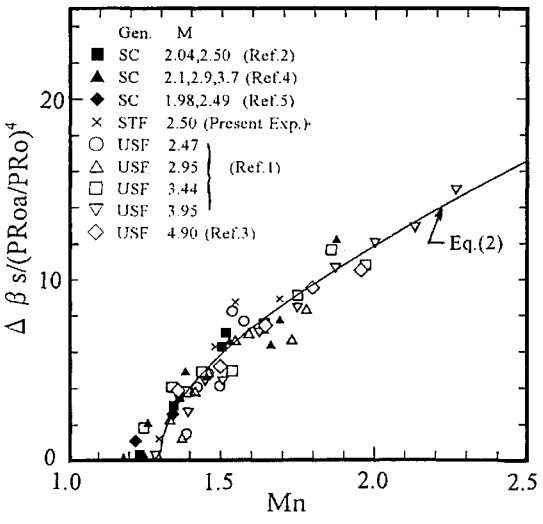

Fig. 4 Improved correlation of the separation angles in terms of overall pressure rise.

deg, and $2.0 \leqq M \leqq 3.5$, the value of PR_{oa} has been shown to be accurately predicted using the equation

$$PR_{oa} = \pi PR_{os}[-0.06865 + 0.2189\xi + 0.2803\xi^2 - 0.05|M - 2.5|(\pi/2 - \xi)]/(2\xi) \quad (1)$$

where PR_{os} is the two-dimensional oblique shock pressure ratio based on a flow-deflection angle of α (cf., PR_o is the shock pressure ratio based on β_o) and ξ is $\tan^{-1}[1/(\sin\alpha \tan\lambda)]$ (in radians; see Fig. 1c). Equation (1) provides values within 3% of the corresponding CFD values.

Each group of data shown in Fig. 3 can be expressed by a hyperbolic function, with each function having a vertex at about 1.3 (intersection between the function and the abscissa of Fig. 3). The angle $\Delta\beta_s$ appears to be approximated by $c_1 M_n^b (M_n^2 - 1.3^2)^{1/2}$, where c_1 is a constant and the power b, which varies with the fin geometry, is 0 for USF and nearly 1 for SC. Using Taylor–Maccoll theoretical values, PR_{oa} for SC has been shown to correlate with $M_n^{2.25}$, and M_n^2 is directly related to PR_o. Hence, PR_{oa}/PR_o is on the order of $M_n^{2.25}/M_n^2 = M_n^{0.25}$. By dividing $\Delta\beta_s$ by $(PR_{oa}/PR_o)^4$, in the case of SC, the hyperbolic function can be simplified as $\Delta\beta_s/(PR_{oa}/PR_o)^4 \sim c_1 M_n (M_n^2 - 1.3^2)^{1/2}/(M_n^{0.25})^4 = c_1(M_n^2 - 1.3^2)^{1/2}$. As shown in Fig. 4, the parameter $\Delta\beta_s/(PR_{oa}/PR_o)^4$ has caused not only SC data but also STF data to approach that of the USF group. Finally, the relationship

$$\Delta\beta_s/(PR_{oa}/PR_o)^4 = 7.8\sqrt{M_n^2 - 1.3^2} \quad (2)$$

(depicted by the solid line in Fig. 4) has been employed to predict the separation angles β_s. The separation angles β_s predicted by Eq. (2) has been shown to be fairly accurate [within 2 deg (1 deg) of the corresponding experimental value for nearly 90% (70%) of the data points in Fig. 4]. This method can provide a rapid and reasonable estimation of the location of primary separation.

Acknowledgment

The authors would like to express their sincere gratitude to F. K. Lu for providing data from tests conducted by himself and his colleagues.

References

[1]Lu, F. K., and Settles, G. S., "Mach Number Effects on Conical Surface Features of Swept Shock-Wave/Boundary-Layer Interactions," *AIAA Journal*, Vol. 28, No. 1, 1990, pp. 91–97.

[2]Deng, X. Y., and Liao, J. H., "Correlation of Conical Interactions Induced by Sharp Fins and Semicones," *AIAA Journal*, Vol. 31, No. 5, 1993, pp. 962, 963.

[3]Rodi, P. E., and Dolling, D. S., "An Experimental/Computational Study of Sharp Fin Induced Shock Wave/Turbulent Boundary Layer Interactions at Mach 5: Experimental Results," AIAA Paper 92-0749, Jan. 1992.

[4]Avduyevskiy, V. S., and Gretsov, V. K., "Investigation of a Three-Dimensional Separated Flow Around Semicones Placed on a Plane Plate," NASA TTF-13578, July 1971.

[5]Saida, N., Ooka, T., and Koide, S., "Interaction Between Shock Waves and Boundary Layer Induced by a Semicone Placed on a Flat Plate," *Journal of the Japan Society for Aeronautical and Space Sciences*, Vol. 33, No. 374, 1985, pp. 159–166 (in Japanese).

[6]Saida, N., Ogata, R., and Koide, S., "Shock Wave/Boundary Layer Interactions Induced by a Rhombic Delta Fin," *Proceedings of the Symposium on Shock Waves*, edited by R. Yamane, Tokyo Inst. of Technology, Tokyo, Japan, 1996, pp. 51–54 (in Japanese).

[7]Koide, S., Griesel, C. J. W., and Stollery, J. L., "Correlation of Shock Angles Caused by Rhombic Delta Wings," *AIAA Journal*, Vol. 34, No. 7, 1996, pp. 1529–1531.

[8]Koide, S., Griesel, C. J. W., and Stollery, J. L., "Effects of Strakes on a Glancing Shock Wave/Turbulent Boundary-Layer Interaction," *Journal of Aircraft*, Vol. 32, No. 5, 1995, pp. 985–992.

Visualization and Analysis of Bow Shocks in a Superorbital Expansion Tube

Margaret Wegener,* Tim McIntyre,†
Halina Rubinsztein-Dunlop,‡ Alexis Bishop,§
Ray Stalker,¶ and Richard Morgan**
University of Queensland, Brisbane 4072, Australia

Nomenclature

M	= Mach number
β	= angle of shock to freestream flow
γ	= ratio of specific heats
δ	= angle included between model and shock
ρ	= density
1	= upstream of shock
2	= downstream of shock

Introduction

SUPERORBITAL expansion tubes are being developed at the University of Queensland to generate flows faster than Earth orbital speeds.[1] They are capable of producing enthalpies far greater than those of existing ground-based testing facilities (free piston-driven shock tunnels and conventional expansion tubes), which enables the aerodynamic study of vehicles designed to return to Earth's atmosphere or enter the atmosphere of other planets.

Accompanying the development of these facilities is the requirement for reliable instrumentation capable of performing measurements within the short test times, typically up to 100 μs. Optical techniques offer this capability, providing nonintrusive measurements recorded over submicrosecond laser pulse durations. One well-established diagnostic method is interferometry, which records gas density variations over the whole field of view in a manner that can be interpreted both qualitatively and quantitatively. A relatively new form is holographic interferometry. In an early practical application to gas dynamics, holographic interferometry was used to study supersonic air flow around cones in a wind tunnel, as described

Received Nov. 20, 1995; accepted for publication Feb. 19, 1996.

*Postgraduate Student, Department of Physics and Department of Mechanical Engineering.

†Research Fellow, Department of Physics.

‡Associate Professor, Department of Physics.

§Postgraduate Student, Department of Physics.

¶Professor, Department of Mechanical Engineering. Associate Fellow AIAA.

**Associate Professor, Department of Mechanical Engineering. Member AIAA.